Adv. Radio Sci., 15, 199–206, 2017
https://doi.org/10.5194/ars-15-199-2017

Advances in
Radio Science
Open Access Proceedings

El Niño influence on the mesosphere/lower thermosphere circulation at midlatitudes as seen by a VHF meteor radar at Collm (51.3° N, 13° E)

Christoph Jacobi[1], **Tatiana Ermakova**[2], **Daniel Mewes**[1], **and Alexander I. Pogoreltsev**[2]

[1]Leipzig Institute for Meteorology, Universität Leipzig, Stephanstr. 3, 04103 Leipzig, Germany
[2]Russian State Hydrometeorological University, St. Petersburg, Russia

Correspondence to: Christoph Jacobi (jacobi@uni-leipzig.de)

Received: 15 November 2016 – Revised: 9 January 2017 – Accepted: 9 January 2017 – Published: 21 September 2017

Abstract. Mesosphere/lower thermosphere (MLT) zonal winds continuously measured by a VHF meteor radar at Collm, Germany (51.3° N, 13.0° E) in the height range 82 – 97 km from 2004 to date are analyzed with respect to the signature of El Niño. The comparison of Niño3 equatorial SST index and MLT wind time series shows that in January and especially in February zonal winds are positively correlated with the Niño3 index. We note a delay of about one month of the MLT zonal wind effect with respect to equatorial sea surface temperature variability. The signal is strong for the upper altitudes (above 90 km) accessible to the radar observations, but weakens with decreasing height. This reflects the fact that during El Niño years the westerly winter middle atmosphere wind jet is weaker, and this is also the case with the easterly lower thermospheric jet. Owing to the reversal of the absolute El Niño signal from negative to positive with altitude, at the height of the maximum meteor flux, which is around 90 km, the El Niño signal is weak. The experimental results can be qualitatively reproduced by numerical experiments using a mechanistic global circulation model with prescribed tropospheric temperatures and latent heat release for El Niño and La Niña conditions.

1 Introduction

Mesosphere/lower thermosphere (MLT) winds and temperatures show considerable variability at time scales of several years, which is at least partly owing to the influence of atmospheric variability below. One of the primary circulation patterns at equatorial latitudes, which also affects climate worldwide is El Niño and its counterpart La Niña. El Niño events are characterised by high central Pacific sea surface temperature (SST), more clouds over the Pacific, and an anomaly of the Walker circulation. They are also connected with a cooling of the equatorial stratosphere and therefore a reduced temperature gradient between lower latitudes and the polar vortex and weakening of the latter. On average the polar stratospheric vortex is weaker during El Niño years than it is during La Niña years. This means that the high-latitude stratosphere is warmer during El Niño years, however, the mesosphere is colder then, which has been also observed by satellites and could also successfully been modelled (Sassi et al., 2004; Garcia-Herrera et al., 2006; Fischer et al., 2008; Lu et al., 2011; Li et al., 2013). El Niño also leads to enhanced probability of major stratospheric warmings (van Loon and Labitzke, 1987; Taguchi and Hartmann, 2006; Camp and Tung, 2007). Major stratospheric warmings are strong disturbances of the stratospheric polar vortex with a reversal of the zonal mean flow.

There has been interest in a possible coupling of El Niño also with the MLT region. Jacobi and Kürschner (2002) found that the correlation between El Niño and zonal wind at 90 km altitude over Collm, Germany (51.3° N, 13° E), is mainly negative in winter, but weakly positive in summer. They used data from 1979–1999. However, Jacobi (2009), using the same dataset extended until 2008 showed that after the 1990s these correlations decrease and even tend to reverse.

Modelling of El Niño influence on the middle atmosphere has mainly been done with focus on the temperature response and wave forcing. From WACCM model runs Li et al. (2013) obtained negative (westward) wave drag in the stratosphere during El Niño, but positive drag in the mesosphere. Conse-

quently this is connected with easterly wind anomalies in the stratosphere, as reported by Taguchi and Hartmann (2006), Fischer et al. (2008) and Lu et al. (2011). The positive wave drag anomaly in the mesosphere reduces this negative wind anomaly. Most models, however, are confined to the stratosphere and mesosphere, or the analyses for the MLT did not focus on the wind.

Here we use observations at Collm made with a VHF meteor radar since 2004, which, in contrast to the earlier analyses by Jacobi and Kürschner (2002) and Jacobi (2009) cover the entire height region between about 80 and 100 km. We also apply the Middle and Upper Atmosphere Model (MUAM), which is a mechanistic circulation model from the ground to the thermosphere to interpret the observations.

2 Meteor radar wind measurements at Collm

At Collm Observatory (51.3° N, 13° E), a SKiYMET meteor radar is operated on 36.2 MHz since summer 2004 (Jacobi, 2012). Original pulse repetition frequency (prf) was 2144 Hz (effectively 536 Hz, due to 4-point coherent integration), power was 6 kW and the transmitting antenna was a 3-element Yagi. The sampling resolution was 1.87 ms. The angular and range resolutions were $\sim 2°$ and 2 km, respectively. The pulse width was 13 µs; the receiver bandwidth was 50 kHz (see also Stober et al., 2012).

The wind measurement principle is the detection of the Doppler shift of the reflected VHF radio waves from ionised meteor trails, which delivers radial wind velocities at the position of the meteor. An interferometer, consisting of five 2-element Yagi antennas arranged as an asymmetric cross was used to detect azimuth and elevation angle from phase comparisons of individual receiver antenna pairs. Together with range measurements the meteor trail position can be detected. The raw data collected consist of azimuth and elevation angle, wind velocity along the line of sight from the receiving antenna to the meteor, meteor height, and additionally the decay time for each single meteor trail. The data collection procedure is also described in detail by Hocking et al. (2001).

The individual meteor trail reflection heights roughly vary between 75 and 110 km, with a maximum around 90 km (e.g. Stober et al., 2008). In the standard configuration used here, the data are binned in 6 different not overlapping height gates centred at 82, 85, 88, 91, 94, and 98 km. Individual winds calculated from the meteors are collected to form half-hourly mean values using a least squares fit of the horizontal wind components to the raw data under the assumption that vertical winds are small (Hocking et al., 2001). An outlier rejection is added. Note that the nominal heights not necessarily correspond to the mean heights within the gates, because the meteors show a vertical distribution with increasing/decreasing count rates with height below/above about 90 km (Stober et al., 2008; Jacobi, 2012). Therefore, below/above 90 km mean heights tend to be higher/lower than nominal heights, and due to the small number of meteors at high altitudes, a substantial difference is visible for 98 km nominal altitude, so that the real mean height is closer to 97 km than 98 km (Jacobi, 2012). For the other height gates, the difference between real and nominal height may be neglected.

Time series of 15-day mean wind parameters have been calculated applying a least-squares regression analysis of 15 days of either zonal or meridional half-hourly horizontal winds on a model wind field including mean wind, diurnal, semidiurnal and terdiurnal oscillation. The results have been attributed to the centre of the 15-day time interval, and then the analysis was repeated by shifting the interval by one day. The 2005–2015 mean seasonal cycles of the zonal and meridional mean wind are shown in Fig. 1. The standard deviation at 88 km calculated from the 11 single years is added as a grey line in the respective panels. The seasonal cycles are similar to those reported earlier e.g. by Jacobi (2012). The left panel of Fig. 1 shows in the lower part the uppermost part of the zonal westerly/easterly wind jets in winter/summer, and in summer part of the lower thermospheric westerly jet above. The wind reversal is connected with the meridional southward jet.

Recently, the Collm radar system has been upgraded, and the main modifications are higher power, a lower prf, and the use of a 4 element transmitting antenna. This effectively increases the number of observed meteors and consequently the height range of wind measurements. The wind analyses, however, are not affected because they rely only on the Doppler shift of the reflected radio waves, and not on meteor parameters.

3 Correlation of MLT winds and El Niño

To compare the variability of MLT zonal winds with El Niño, we use the Niño3 index, which represents the normalized area averaged SST in the region from 5° S–5° N and 150–90° W. We use SST from NOAA Extended Reconstructed Sea Surface Temperature (ERSSTA, Huang et al., 2015), Version 4, normalized to 1981–2010 (KNMI, 2016). There are several indices available that can be used for definition of El Niño (e.g. Trenberth, 1997). The Niño3 index represents the sea surface temperature in the eastern part of the Pacific. The different indices are strongly correlated and the results should not differ qualitatively if another index would be used.

Time series of 15-day mean zonal wind anomalies over Collm at 94 and 85 km, together with smoothed Niño3 indices, are shown in Fig. 2. The wind anomalies have been calculated by simply subtracting the long-term seasonal cycle shown in Fig. 1 from the 15-day analyses. The winters 2006/07, 2009/10, and in particular 2015/16 were characterised by El Niño events. The upper panel of Fig. 2 shows that these events have been accompanied by positive zonal

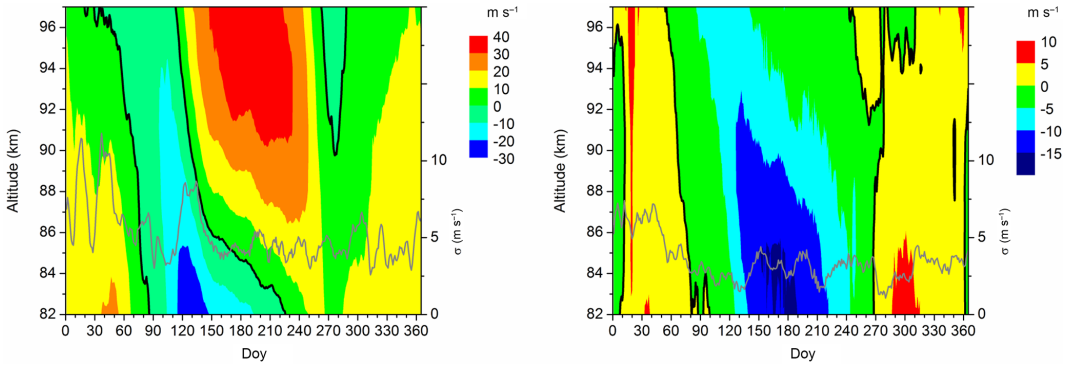

Figure 1. 2005–2015 mean seasonal cycles of the zonal (left) and meridional (right) mean wind. The long-term means are constructed from 15-day mean wind analyses during each year. The black contour line shows the zero wind line. Note the different scaling of the panels. The grey lines show the standard deviations of the 15-day mean analyses at 88 km for each day of the year constructed from 11 years of data, indicating interannual variability.

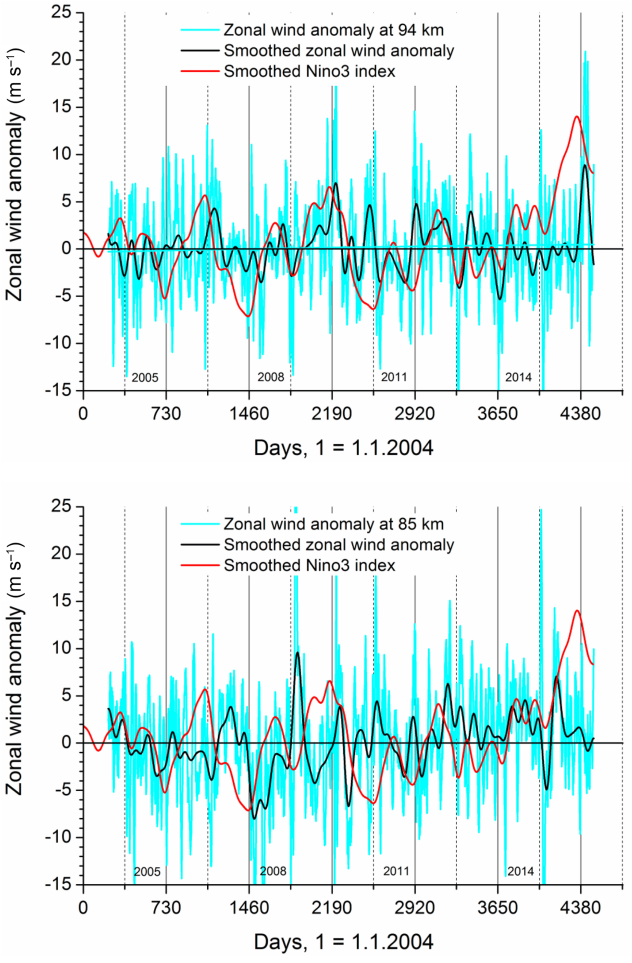

Figure 2. Time series of 15-day mean zonal wind anomalies over Collm (cyan lines) and values smoothed by applying a 45-pt FFT filter (black lines) at 94 km (upper panel) and 85 km (lower panel). Smoothed Niño3 indices are added as red lines.

wind anomalies, while at 85 km such a connection is not visible and there is even a tendency for a negative correlation of MLT zonal wind and Niño3 index.

The strong El Niño event 2015/16 was connected with the strongest zonal winds at 94 km within our record. The moderate El Niño 2009/10 was connected with the 2nd strongest winds, but the weaker event 2005/06, although accompanied by a zonal wind anomaly maximum the early following year, did not result in extraordinarily strong zonal winds. Therefore, there is a tendency that especially strong El Niño events have an effect on the MLT winds, but with only three El Niño events it is not possible to draw substantial conclusions on the effect of weaker events on the MLT.

Garfinkel and Hartmann (2008, 2010) have shown that the effect of El Niño on the polar vortex is stronger for the west phase than for the east phase of the equatorial Quasi-Biennial Oscillation (QBO). Calvo et al. (2009) noted from simulations that El Niño modifies the effect of the QBO on the polar vortex. In our MLT wind record, however, the three El Niño events investigated here were characterised by different QBO phases, and we can, based on the short time series, not draw conclusions on a possible effect on the MLT.

Correlation coefficients of monthly mean Niño3 index and MLT zonal wind at different altitudes were calculated for each month and each radar altitude gate, and the results are shown in Fig. 3. The monthly wind data have been calculated in the same manner than the 15-day means above, but using 28–31 days of half-hourly means, depending on the length of the respective month. The strongest El Niño response is seen in February for the upper height gates. The effect decreases with decreasing altitude and even reverses for the lowest height gates. During the other months of the year the correlation is weaker. The results for winter are in correspondence with literature results. The middle atmosphere zonal winds during El Niño are weakened, but the positive wave drag in the mesosphere reduces this effect with increasing

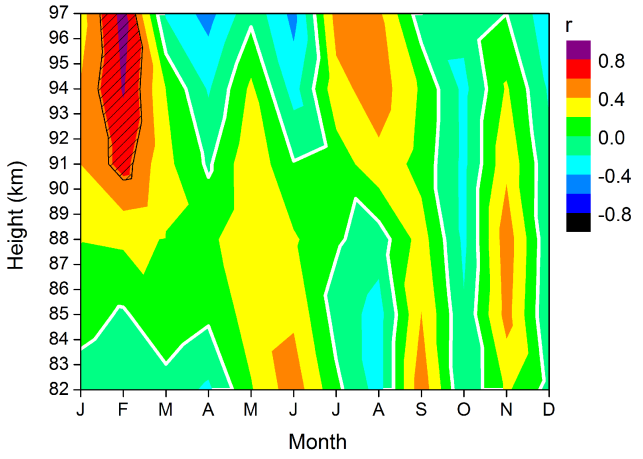

Figure 3. Correlation coefficients of monthly mean zonal winds at different heights and Niño3 indices. Data from August 2004–July 2016 have been used. Significant values at the 5 % level according to a t test are hatched.

altitude, and eventually will lead to the reversal that can be observed in the Collm measurements.

4 MUAM circulation model results

In order to substantiate the observed correlation, we use the MUAM model to simulate the MLT response to El Niño. MUAM is a nonlinear primitive equation 3-D grid point mechanistic model with a resolution of $5° \times 5.625°$ in the horizontal and 56 vertical layers expressed in log-pressure height $z = -H\ln(p/p_0)$ with a constant scale height $H = 7\,\mathrm{km}$ and $p_0 = 1000\,\mathrm{hPa}$. The vertical layers are spaced evenly with a step size $\Delta z = 0.4 \cdot H$. Further details can be obtained from Pogoreltsev et al. (2007).

Heating of the atmosphere due to absorption of solar radiation by water vapor, CO_2, ozone, oxygen and nitrogen is introduced in the model (Fröhlich et al., 2003). Infrared cooling of CO_2 is parameterized after Fomichev et al. (1998), while ozone infrared cooling in the 9.6 µm band is calculated after Fomichev and Shved (1985). Gravity waves in the middle atmosphere are parameterized based on an updated linear Lindzen (1981) scheme. For the thermosphere, an approach after Yigit et al. (2008) is chosen, which especially accounts for the conditions in the thermosphere such as molecular viscosity, thermal conduction, ion friction, and radiative damping in the form of the Newtonian cooling. Thermosphere results are, however, not considered here.

To consider the El Niño influence on the dynamical processes in the extra-tropical middle atmosphere, a semi-empirical parameterization of the latent heat release has been included that takes into account diurnal and longitudinal variations. Latent heating composites for Northern Hemisphere January under El Niño and La Niña conditions have been calculated using MERRA (Rienecker et al., 2011) reanalysis precipitation data. The corresponding composites of geopotential height and temperature at the lower boundary have been constructed from JRA-55 (Kobayashi et al., 2015) reanalyses. The El Niño and La Niña composites have been constructed from 9 strong or moderate events each. The January 2010 fields thus were included in the El Niño composite, but not January 2007. The recent 2015/16 El Niño also has not been included so that only one El Niño event was both included in the composite and covered by the observations. Regarding La Niña, January 2008 and January 2011 fields have been included in the composite, and 7 more cases that for earlier years when radar observations were not available. We therefore expect that, while the overall behaviour of zonal winds in our observations might be reproduced by the model, there will be differences in detail. Ensemble runs consisting of 10 members for El-Niño and La-Niña conditions, respectively, have been performed and ensemble means and their standard deviations have been calculated.

We performed model runs for January conditions. Figure 2 shows that the Niño3 index peaks near the end of the years 2006, 2008, and 2015, while the zonal wind maximises in January or February of the following year, so that there is a delay in MLT response to El Niño. However, with MUAM we are modelling quasi-stationary cases, so that using January conditions represents a compromise between the delayed response and the stationary modelling approach.

January mean zonal mean latitude-log-pressure height cross-sections of temperature and zonal wind as simulated with MUAM for El Niño conditions are shown in Fig. 4. The latitude-height structure reproduces observed features known e.g. from empirical climatologies like CIRA86 (Fleming et al., 1990), URAP (Swinbank and Ortland, 2003) or the radar based GEWM (Portnyagin et al., 2004). At 50–55° N there is a wind reversal from the mesospheric westerly jet to the lower thermosphere easterly jet at about 90 km, which is a little bit lower than observed.

The mean differences between El Niño and La Niña years are shown in Fig. 5. The temperatures on the left panel show the stratospheric warming and mesospheric cooling during El Niño years known from global observations and other models (Sassi et al., 2004; Garcia-Herrera et al., 2006; Fischer et al., 2008; Lu et al., 2011; Li et al., 2013). The reduced stratospheric wind jet reported in the literature (Taguchi and Hartmann, 2006; Fischer et al., 2008; Lu et al., 2011) is shown in the right panel of Fig. 5, and above that in the MLT an increase of the zonal wind is visible. This qualitatively reproduces the Collm observations.

It has to be noted that Fig. 5 shows zonal mean values which are compared with local observations. However, in the presence of stationary planetary waves the local mean winds can differ from the zonal mean. Figure 6 shows in the left panel a longitude-height plot of modelled zonal winds at 52.5° N, which is the MUAM grid point closest to the Collm observations, together with their standard deviations for El Niño conditions. There is an obvious stationary planetary

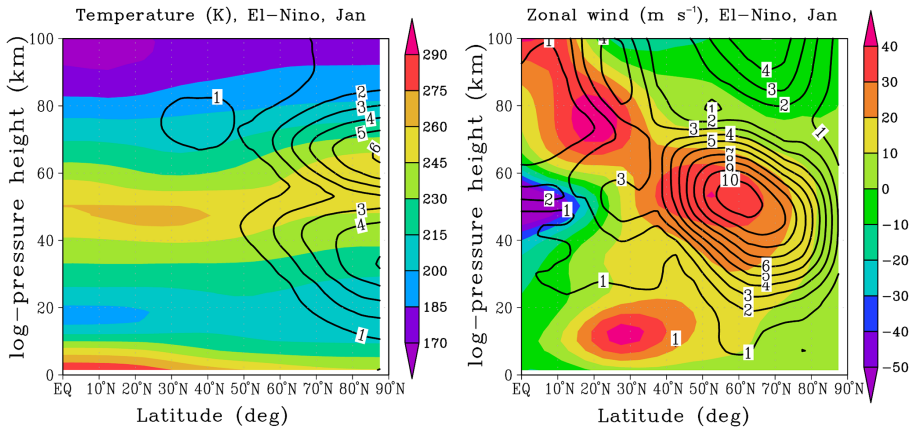

Figure 4. January mean temperatures (left) and zonal winds (right) as simulated with MUAM for El Niño conditions. Colour coding shows mean values over 10 ensemble runs. Standard deviations of the ensemble members are added as black contour lines.

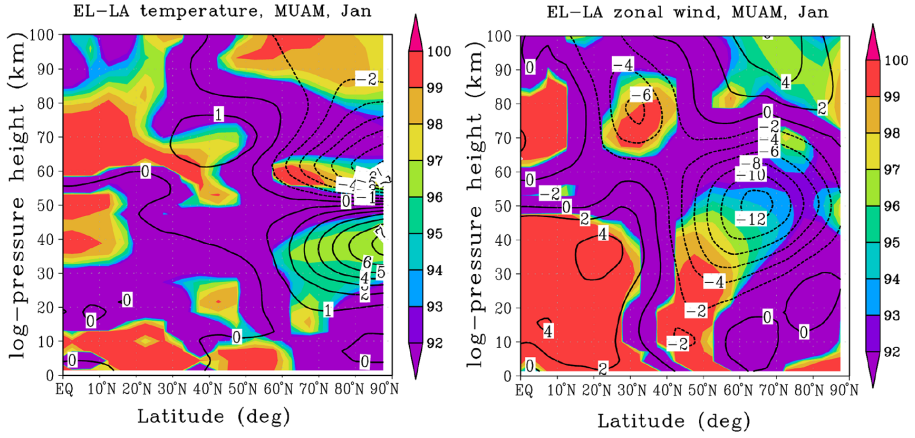

Figure 5. El Niño – La Niña differences of January mean temperature (left) and zonal wind (right) as simulated with MUAM (contour lines). The colour coding shows the significance of the differences according to a t test.

wave mainly expressed near the stratopause but also visible near the mesopause. The right panel of Fig. 6 shows the differences between El Niño and La Niña years at 52.5° N. This plot shows that the differences vary with longitude, broadly in phase with the zonal wind, and that they may even reverse sign. At 13° E one can see that actually in the stratosphere and lower mesosphere the zonal winds during La Niña are weaker than during El Niño, opposite to the behaviour of the zonal mean. However, near the stratopause and above the interannual variability during El Niño years is larger than the El Niño – La Niña differences, so that the local results obviously depend on the years under consideration. The differences between local observations and model results therefore are owing to the fact that mainly different events were investigated and only one El Niño and two La Niña events have been included in both observations and modelling.

In the MLT region one can see that the El Niño – La Niña differences also depend on longitude and may differ in sign. This may be an explanation for changes in the MLT response that has been noted by Jacobi (2009).

5 Lagged correlations

The El Niño signature propagates to the midlatitude middle atmosphere through planetary waves and model results have shown that the strongest signature at high latitudes is few months after the warm event (Garcia-Herrara et al., 2006). This is visible from the Collm observations also (see Fig. 2), and the maximum westerly winds at 94 km occur a few weeks after the Niño3 index peaks. For illustration, Fig. 7 shows lagged correlation of Collm MLT winds on 31 January and Niño3 indices at 94 and 85 km. The MLT wind response maximises about one month after the peak warming event. The correlation maximises at a lag of 32 days with a correlation coefficient of 0.76, which is significant at the 1 % level. At 85 km, the signal is weaker than at 94 km, and the correla-

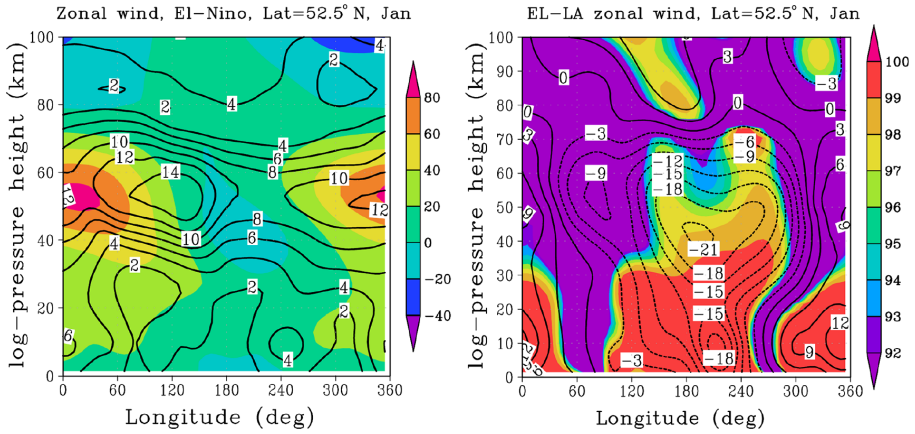

Figure 6. Longitude-height cross-section of January mean zonal winds (left panel) at 52.5° N as simulated with MUAM for El Niño conditions. Colour coding shows mean values over 10 ensemble runs. Standard deviations of the ensemble members are added as black contour lines. On the right panel El Niño – La Niña differences of January mean zonal winds are shown as contour lines. The colour coding shows the significance of the differences according to a *t* test.

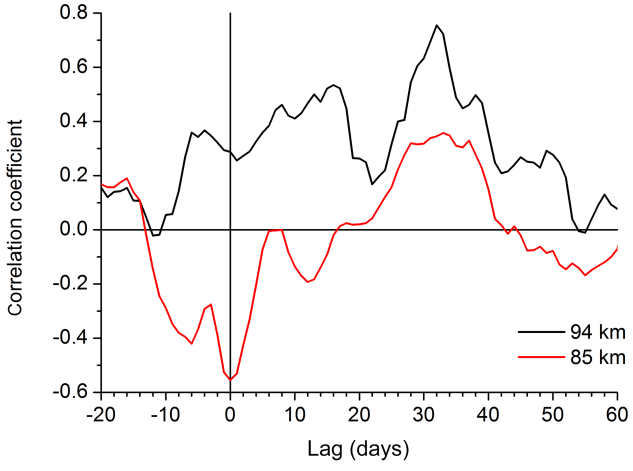

Figure 7. Lagged correlation coefficients of 15-day mean zonal winds over Collm centred around 31 January and Niño3-indices. Positive values denote Collm wind variations lagging the Niño3 index ones. Data used are from 2005–2016.

tion is not significant. At zero lag it is negative, although not significant.

6 Conclusions

Radar observations of winds over Collm have shown that the zonal wind in the MLT region in February is correlated with the Eastern Pacific SST. In the upper mesosphere, the effect reduces and there is a tendency that it even reverses, although the effect is not significant at 82 km. The Collm observations also show a delay of the MLT wind response with respect to the peak Pacific SST warming, in correspondence with literature (Garcia-Herrara et al., 2006).

The decrease of the correlation in the upper mesosphere is in correspondence with MUAM model analyses that show that the negative zonal wind response in the stratosphere and mesosphere is reversed in the MLT. This result is, however, only true for the zonal mean. Locally the middle atmosphere wind response differs and the local model results at the coordinates of Collm are not supported the observations. However, the model runs for El Niño – La Niña are based on composite years mainly different from the ones of the observations and the interannual variability is strong also for different El Niño cases.

Earlier reports on El Niño effects on the MLT often has used observations at about 90 km (e.g. Jacobi, 2009). At this altitude, however, the response of the zonal wind to El Niño is weak (correlation coefficient of about 0.5 in February, see Fig. 3). In addition, the model results (Fig. 5, right panel) show that the response depends on latitude and therefore may change when the stationary planetary waves change.

7 Code availability

MUAM model code is available from the authors upon request.

8 Data availability

Collm MLT wind data are available from the corresponding author upon request. Niño3 indices have been provided by KNMI through the KNMI climate explorer, https://climexp.knmi.nl.

Acknowledgements. Niño3 indices based on NOAA ERSST.v4 seas surface temperatures have been kindly provided by KNMI through the KNMI climate explorer, https://climexp.knmi.nl. Ch. Jacobi and D. Mewes acknowledge support by the SFB/TR 172 in Project D01 funded by the Deutsche Forschungsgemeinschaft (DFG). MUAM model simulations were supported by the Russian Science Foundation through grant number 14-17-00685.

Edited by: M. Förster
Reviewed by: two anonymous referees

References

Calvo, N., Giorgetta, M. A., Garcia-Herrera, R., and Manzini, E.: Nonlinearity of the combined warm ENSO and QBO effects on the Northern Hemisphere polar vortex in MAECHAM5 simulations, J. Geophys. Res., 114, D13109, https://doi.org/10.1029/2008JD011445, 2009.

Camp, C. D. and Tung, K.-K.: Stratospheric polar warming by ENSO in winter: A statistical study, Geophys. Res. Lett., 34, L04809, https://doi.org/10.1029/2006GL028521, 2007.

Fischer, A. M., Shindell, D. T., Winter, B., Bourqui, M. S., Faluvegi, G., Rozanov, E., Schraner, M., and Brönnimann, S.: Stratospheric winter climate response to ENSO in three chemistry-climate models, Geophys. Res. Lett., 35, L13819, https://doi.org/10.1029/2008GL034289, 2008.

Fleming, E. L., Chandra, S., Barnett, J. J., and Corney, M: Zonal mean temperature, pressure, zonal wind and geopotential height as function of latitude, Adv. Space. Res., 10, 11–59, 1990.

Fomichev, V. I. and Shved, G. M.: Parameterization of the radiative flux divergence in the 9.6 µm O_3 band, J. Atmos. Terr. Phys., 47, 1037–1049, https://doi.org/10.1016/0021-9169(85)90021-2, 1985.

Fomichev, V. I., Blanchet, J.-P., and Turner, D. S.: Matrix parameterization of the 15 µm CO_2 band cooling in the middle and upper atmosphere for variable CO_2 concentration, J. Geophys. Res., 103, 11505–11528, https://doi.org/10.1029/98JD00799, 1998.

Fröhlich, K., Pogoreltsev, A., and Jacobi, Ch.: The 48 Layer COMMA-LIM Model: Model description, new aspects, and Climatology, Rep. Inst. Meteorol. Univ. Leipzig, 30, 157–185, 2003.

Garcia-Herrera, R., Calvo, N., Garcia, R. R., and. Giorgetta, M. A: Propagation of ENSO temperature signals into the middle atmosphere: A comparison of two general circulation models and ERA-40 reanalysis data, J. Geophys. Res., 111, D06101, https://doi.org/10.1029/2005JD006061, 2006.

Garfinkel, C. I. and Hartmann, D. L.: Different ENSO teleconnections and their effects on the stratospheric polar vortex, J. Geophys. Res., 113, D18114, https://doi.org/10.1029/2008JD009920, 2008.

Garfinkel, C. I. and Hartmann, D. L.: Influence of the quasi-biennial oscillation on the North Pacific and El Niño teleconnections, J. Geophys. Res., 115, D20116, https://doi.org/10.1029/2010JD014181, 2010.

Hocking, W. K., Fuller, B., and Vandepeer, B.: Real-time determination of meteor-related parameters utilizing modern digital technology, J. Atmos. Solar-Terr. Phys., 63, 155–169, https://doi.org/10.1016/S1364-6826(00)00138-3, 2001.

Huang, B., Banzon, V. F., Freeman, E., Lawrimore, J., Liu, W., Peterson, T. C., Smith, T. M., Thorne, P. W., Woodruff, S. D., and Zhang, H.-M.: Extended Reconstructed Sea Surface Temperature version 4 (ERSST.v4): Part I. Upgrades and intercomparisons, J. Clim., 28, 911–930, https://doi.org/10.1175/JCLI-D-14-00006.1, 2015.

Jacobi, Ch.: Possible signal of tropospheric circulation patterns in middle atmosphere dynamics, Collm (51.3° N, 13° E) mesosphere lower thermosphere winds 1979–2008, Rep. Inst. Meteorol. Univ. Leipzig, 45, 153–162, 2009.

Jacobi, Ch.: 6 year mean prevailing winds and tides measured by VHF meteor radar over Collm (51.3° N, 13.0° E), J. Atmos. Sol.-Terr. Phys., 78–79, 8–18, https://doi.org/10.1016/j.jastp.2011.04.010, 2012.

Jacobi, Ch. and Kürschner, D.: A possible connection of midlatitude mesosphere/lower thermosphere zonal winds and the Southern Oscillation, Phys. Chem. Earth, 27, 571–577, https://doi.org/10.1016/S1474-7065(02)00039-6, 2002.

KNMI: KNMI climate explorer, available at: https://climexp.knmi.nl, downloaded: 27 May 2016.

Kobayashi, S., Ota, Y., Harada, Y., Ebita, A., Moriya, M., Onoda, H., Onogi, K., Kamahori, H., Kobayashi, C., Endo, H., Miyaoka, K., and Takahashi, K.: The JRA-55 Reanalysis: General specifications and basic characteristics, J. Meteorol. Soc. Japan, 93, 5–48, https://doi.org/10.2151/jmsj.2015-001, 2015.

Li, T., Calvo, N., Yue, J., Dou, X., Russell III, J. M., Mlynczak, M. G., She, C.-Y., and Xue, X.: Influence of El Niño-Southern Oscillation in the mesosphere, Geophys. Res. Lett., 40, 3292–3296, https://doi.org/10.1002/grl.50598, 2013.

Lindzen, R. S.: Turbulence and stress owing to gravity wave and tidal breakdown, J. Geophys. Res., 86, 9707–9714, https://doi.org/10.1029/JC086iC10p09707, 1981.

Lu, C., Liu, Y., and Liu, C.: Middle atmosphere response to ENSO events in Northern Hemisphere winter by the Whole Atmosphere Community Climate Model, Atmos.-Ocean, 49, 95–111, https://doi.org/10.1080/07055900.2011.576451, 2011.

Pogoreltsev, A. I., Vlasov, A. A., Fröhlich, K., and Jacobi, Ch.: Planetary waves in coupling the lower and upper atmosphere, J. Atmos. Sol.-Terr. Phys., 69, 2083–2101, https://doi.org/10.1016/j.jastp.2007.05.014, 2007.

Portnyagin, Yu., T. Solovjova, T., Merzlyakov, E., Forbes, J., Palo, S., Ortland, D., Hocking, W., MacDougall, J., Thayaparan, T., Manson, A., Meek, C., Hoffmann, P., Singer, W., Mitchell, N., Pancheva, D., Igarashi, K., Murayama, Y., Jacobi, Ch., Kürschner, D., Fahrutdinova, A., Korotyshkin, D., Clark, R., Tailor, M., Franke, S., Fritts, D., Tsuda, T., Nakamura, T., Gurubaran, S., Rajaram, R., Vincent, R., Kovalam, S., Batista, P., Poole, G., Malinga, S., Fraser, G., Murphy, D., Riggin, D., Aso, T., and Tsutsumi, M.: Mesosphere/lower thermosphere prevailing wind model, Adv. Space Res., 34, 1755–1762, https://doi.org/10.1016/j.asr.2003.04.058, 2004.

Rienecker, M. M., Suarez, M. J., Gelaro, R., Todling, R., Bacmeister, J., Liu, E., Bosilovich, M. G., Schubert, S. D., Takacs, L., Kim, G.-K., Bloom, S., Chen, J., Collins, D., Conaty, A., da Silva, A., Gu, W., Joiner, J., Koster, R. D., Lucchesi, R., Molod, A., Owens, T., Pawson, S., Pegion, P., Redder, C. R., Reichle, R., Robertson, F. R., Ruddick, A. G., Sienkiewicz, M., and Woollen, J.: MERRA: NASA's Modern-Era Retrospective Anal-

ysis for Research and Applications, J. Climate, 24, 3624–3648, https://doi.org/10.1175/JCLI-D-11-00015.1, 2011.

Sassi, F., Kinnison, D., Boville, B. A., Garcia, R. R., and Roble, R.: Effect of El Niño–Southern Oscillation on the dynamical, thermal, and chemical structure of the middle atmosphere, J. Geophys. Res., 109, D17108, https://doi.org/10.1029/2003JD004434, 2004.

Stober, G., Jacobi, Ch., Fröhlich, K., and Oberheide, J.: Meteor radar temperatures over Collm (51.3° N, 13° E), Adv. Space Res., 42, 1253–1258, https://doi.org/10.1016/j.asr.2007.10.018, 2008.

Stober, G., Jacobi, Ch., Matthias, V., Hoffmann, P., and Gerding, M.: Neutral air density variations during strong planetary wave activity in the mesopause region derived from meteor radar observations, J. Atmos. Sol.-Terr. Phys., 74, 55–63, https://doi.org/10.1016/j.jastp.2011.10.007, 2012.

Swinbank, R. and Ortland, D. A.: Compilation of wind data for the Upper Atmosphere Research Satellite (UARS) Reference Atmosphere Project, J. Geophys. Res., 108, 4615, https://doi.org/10.1029/2002JD003135, 2003.

Taguchi, M. and Hartmann, D. L.: Increased occurrence of stratospheric sudden warmings during El Niño as simulated by WACCM, J. Clim., 19, 324–332, https://doi.org/10.1175/jcli3655.1, 2006.

Trenberth, K. E.: The definition of El Niño, B. Am. Meteorol. Soc., 78, 2771–2777, https://doi.org/10.1175/1520-0477(1997)078<2771:TDOENO>2.0.CO;2, 1997.

van Loon, H. and Labitzke, K.: The Southern Oscillation. Part V: The anomalies in the lower stratosphere of the northern hemisphere in winter and a comparison with the quasi-biennial oscillation, Mon. Weather Rev., 115, 357–369, https://doi.org/10.1175/1520-0493(1987)115<0357:TSOPVT>2.0.CO;2, 1987.

Yigit, E., Aylward, A. D., and Medvedev, A. S.: Parameterization of the effects of vertically propagating gravity waves for thermosphere general circulation models: Sensitivity study, J. Geophys. Res., 113, D19106, https://doi.org/10.1029/2008JD010135, 2008.